Int. J. Heat Mass Transfer. Vol. 36, No. 9, pp. 2293–2303, 1993
Printed in Great Britain

0017-9310/93 $6.00+0.00

Vapor flow analysis of an axially rotating heat pipe

A. FAGHRI, S. GOGINENI and S. THOMAS
Department of Mechanical and Materials Engineering, Wright State University, Dayton, OH 45435 U.S.A.

(*Received* 29 *June* 1992 *and in final form* 2 *November* 1992)

Abstract—The vapor flow in an axially rotating heat pipe has been numerically analyzed using a two-dimensional axisymmetric model in cylindrical coordinates. A parametric study was conducted for radial Reynolds numbers of 0.01, 4.0, and 20.0, and rotational speeds ranging from 0 to 2800 r.p.m. The numerical results indicate that the pressure and the axial, radial, and tangential velocities are significantly affected by the rotational speed and the radial Reynolds number. In comparison to non-rotating heat pipes, the radial pressure distribution is no longer uniform. Also, above a certain rotational speed, flow reversal occurs near the centerline of the heat pipe. The shear stress components in the axial and tangential directions at the inner pipe wall increase with the evaporation rate and the rotational speed. The magnitude of the shear stress components are highest in the condenser section. The results of this study will be beneficial in the prediction of the performance of axially rotating heat pipes.

INTRODUCTION

HEAT PIPES transport heat energy over large distances with relatively low temperature drops and no external power requirements [1]. A heat pipe is a closed container, within which is a thin, liquid-saturated wick structure attached to the pipe wall. Heat transfer occurs by evaporation of the fluid from the wick structure in the evaporator section. The vapor travels to the condenser section due to a pressure gradient in the vapor. The vapor then condenses onto the wick in the condenser, releasing the latent heat of vaporization to the ultimate heat sink. The condensate returns to the evaporator by capillary forces within the wick structure to repeat the process. Wickless rotating heat pipes have been studied where the heat pipe rotates about its longitudinal axis. The rotating heat pipe concept was formulated originally by Gray [2] as an improved version of the conventional heat pipe for specific applications where gravity and acceleration limitations must be overcome. The rotating heat pipe does not contain a wick structure, but relies solely on centrifugal forces to transport the liquid from the condenser to the evaporator. The rotating heat pipe is of significant interest for applications such as cooling electric motors, turbine blades, machine tools, bearings and other rotating mechanical devices [3–5].

Faghri and Parvani [6] and Chen and Faghri [7] numerically solved the complete two-dimensional, laminar, steady conservation of mass, momentum, and energy equations with and without the effect of the wall and the wick for conventional and annular nonrotating heat pipes.

Previous investigations concerning axially rotating heat pipes generally analyzed the condensation within the condenser section using the Nusselt analysis. Daniels and Al-Jumaily [8] analyzed the condensate flow in the condenser section of an axially rotating heat pipe with a slight internal taper. The analysis originally derived by Nusselt [9] for the gravity-driven laminar flow of condensate of pure vapors was followed to obtain the heat transfer rate. Since the friction coefficient at the vapor–liquid interface was unknown, it was assumed to be $f = 16/Re$ or $0.0791/Re^{0.25}$ for laminar or turbulent vapor flow. It was found that the performance of rotating heat pipes could be improved by increasing the taper angle, the length of the condenser, and the volume of working fluid within the pipe.

Marto [10] performed an analysis similar to that of Daniels and Al-Jumaily [8] for the heat transfer within the condenser of an axially rotating heat pipe. The analysis by Marto included the effect of the vapor pressure drop in the condenser, but neglected the momentum effect of the condensing vapor when considering the interfacial shear stress. Again, the friction factor had to be assumed as was done by Daniels and Al-Jumaily. Marto concluded that the heat transfer rate increased approximately as the square root of the rotational speed, when the resistances of the wall and the outside convection were neglected. Marto also concluded that the performance of rotating heat pipes could be improved by using thin-walled condensers made of high conductivity materials.

Daniels and Al-Baharnah [11] analytically predicted the condenser wall temperature profile, including the effects of the concentration of noncondensible gas, the type of working fluid, the condenser wall material, and the cooling medium. The conservation equations for mass, axial and radial momentum, and energy in the condensate film were derived. In the analysis, the velocity gradient in the circumferential direction and the shear force at the vapor–liquid film interface were neglected. Results of the analysis were compared to experimental data with good agreement.

Salinas and Marto [12] employed a two-dimen-

NOMENCLATURE

$C_{f,rz}$	coefficient of friction in the r–z direction, $2\tau_{rz,w}/\rho\overline{W}^2$
$C_{f,r\theta}$	coefficient of friction in the r–θ direction, $2\tau_{r\theta,w}/\rho U_w^2$
D	inner diameter of the rotating heat pipe [m]
h_{fg}	heat of vaporization [J kg^{-1}]
L	length of the rotating heat pipe [m]
L_a	length of the adiabatic section [m]
L_c	length of the condenser section [m]
L_e	length of the evaporator section [m]
N	rotational speed [r.p.m.]
p	pressure [N m^{-2}]
p_0	vapor pressure at the evaporator end cap [N m^{-2}]
p^*	dimensionless pressure, $(p-p_0)/\rho\overline{W}^2$
Q	local heat rate per unit length [W m^{-1}]
r	radial coordinate [m]
R	inner radius of the rotating heat pipe [m]
r^+	normalized radial distance, r/R
Re	axial Reynolds number, $\overline{W}D/\nu$
Re_r	radial Reynolds number, V_wR/ν
Re_ϕ	rotational Reynolds number, U_wD/ν
Ro	Rossby number, $V_w/\omega R$
u	tangential component of velocity [m s^{-1}]
U_w	tangential velocity of the inner pipe wall, $R\omega$ [m s^{-1}]
u^+	normalized tangential velocity, u/U_w
v	radial component of velocity [m s^{-1}]
V_w	radial blowing or suction velocity at the inner radius of the pipe [m s^{-1}]
v^+	normalized radial velocity, v/V_w
w	axial component of velocity [m s^{-1}]
$\overline{W}$	mean axial velocity in the adiabatic section [m s^{-1}]
W_{avz}	mean axial velocity at any z location [m s^{-1}]
w^+	normalized axial velocity, w/W_{avz}
z	axial coordinate [m]
z^*	dimensionless axial distance, z/R
z^+	normalized axial distance, z/L.

Greek symbols

Γ	swirl ratio, $U_w/\overline{W}$
θ	tangential coordinate [rad]
μ	absolute viscosity [kg m^{-1} s^{-1}]
ν	kinematic viscosity [m^2 s^{-1}]
ρ	density [kg m^{-3}]
$\tau_{rz,w}$	shear stress at the wall in the r–z direction [N m^{-2}]
$\tau_{r\theta,w}$	shear stress at the wall in the r–θ direction [N m^{-2}]
ω	angular velocity [rad s^{-1}].

Subscripts

a	adiabatic section
c	condenser section
e	evaporator section
w	at the wall.

sional numerical model to analyze the conjugate heat conduction within an axially rotating heat pipe. Internal triangular fins, which enhance the heat transfer coefficient, were analyzed using the finite-element method of solution. The local condensate velocity and thickness in the troughs between the fins were derived using a Nusselt-type analysis, where the interfacial shear between the vapor and the liquid was neglected. The rotational speed was varied from 1000 to 15000 r.p.m., the number of fins varied from 1 to 400, and three heat transfer coefficients, 5.70, 28.4, and 284 kW m^{-2} K^{-1}, were specified at the outer radius of the pipe. It was determined that two-dimensional heat conduction affects the local heat flux distribution within the fins, condensate, and the wall. The authors state that an optimum fin configuration can be derived for a given set of operating conditions, working fluid, wall material, and outside heat rejection method.

All of the previous investigations of rotating heat pipes used a Nusselt-type analysis in the condenser section, where either the friction coefficient at the vapor–liquid interface was estimated empirically, or it was assumed to be negligible. This assumption may be invalid for small-diameter heat pipes operating under large heat loads [12]. In these cases, it is important that the shear stress profiles along the heat pipe be known. Also, the heat pipe should be solved as a single-domain problem, instead of considering only the condenser section. To the knowledge of the authors, there is no study available related to the vapor flow in axially rotating heat pipes. Therefore, the objective of the present study is to analyze the vapor flow within a heat pipe rotating about its longitudinal axis as a single-domain problem by numerically solving the two-dimensional axisymmetric differential equations conserving mass and momentum. The effects of the radial Reynolds number and the rotational speed are determined by a parametric study. Pressure, velocity, and shear stress profiles along the entire length of the rotating heat pipe are given to understand and quantify the fundamental hydrodynamic phenomena occurring within the vapor flow of the rotating heat pipe. The information obtained from this study will be beneficial in predicting the heat transfer characteristics of axially rotating heat pipes, since the shear stress at the vapor–

liquid interface will be known. This analysis will provide the needed information so that the analytical models mentioned above can be improved.

MATHEMATICAL FORMULATION

The problem under consideration is a circular cross section heat pipe with sealed ends rotating about its longitudinal axis with a constant angular velocity ω, as shown in Fig. 1. The lengths of the evaporator, adiabatic, and condenser sections are $L_e = 0.2$ m, $L_a = 0.6$ m, and $L_c = 0.2$ m. The inner diameter of the heat pipe studied is $D = 0.02$ m. The working fluid is water vapor at 100 C. Evaporation and condensation within the heat pipe are modeled as blowing and suction at the inner wall of the pipe. The evaporation and condensation are considered to be uniform around the circumference of the pipe and along the lengths of the evaporator and condenser sections. Therefore, the two-dimensional axisymmetric cylindrical coordinate system is used. It is assumed that the fluid properties are constant, and the flow is laminar, steady, and incompressible. The gravitational body force and viscous dissipation are assumed to be negligible. The differential equations conserving mass and momentum for this case are [13]:

Mass:

$$\frac{1}{r}\frac{\partial}{\partial r}(rv)+\frac{\partial w}{\partial z}=0 \tag{1}$$

r direction momentum:

$$\rho\left(v\frac{\partial v}{\partial r}-\frac{u^2}{r}+w\frac{\partial v}{\partial z}\right)=-\frac{\partial p}{\partial r}+\mu\left[\frac{\partial}{\partial r}\left(\frac{1}{r}\frac{\partial}{\partial r}(rv)\right)+\frac{\partial^2 v}{\partial z^2}\right] \tag{2}$$

θ direction momentum:

$$\rho\left(v\frac{\partial u}{\partial r}+\frac{vu}{r}+w\frac{\partial u}{\partial z}\right)=\mu\left[\frac{\partial}{\partial r}\left(\frac{1}{r}\frac{\partial}{\partial r}(ru)\right)+\frac{\partial^2 u}{\partial z^2}\right] \tag{3}$$

z direction momentum:

$$\rho\left(v\frac{\partial w}{\partial r}+w\frac{\partial w}{\partial z}\right)=-\frac{\partial p}{\partial z}+\mu\left[\frac{1}{r}\frac{\partial}{\partial r}\left(r\frac{\partial w}{\partial r}\right)+\frac{\partial^2 w}{\partial z^2}\right]. \tag{4}$$

At the inner wall of the heat pipe ($r = R$), the no-slip condition for the axial and tangential velocities is in effect

$$u(R, z) = U_w = R\omega \tag{5}$$

$$w(R, z) = 0. \tag{6}$$

Evaporation and condensation at the inner wall of the heat pipe are modeled as uniform blowing and suction

$$v(R, z) = \begin{cases} -V_w, & 0 \leqslant z \leqslant L_e \quad \text{(Evaporator)} \quad (7a) \\ 0, & L_e \leqslant z \leqslant L_e + L_a \quad \text{(Adiabatic)} \quad (7b) \\ V_w, & L_e + L_a \leqslant z \leqslant L \quad \text{(Condenser).} \quad (7c) \end{cases}$$

The blowing and suction velocities are related to the local heat rate per unit length as:

$$V_w = \frac{Q}{\pi D \rho h_{fg}}. \tag{8}$$

At the end caps of the heat pipe ($z = 0, L$), the radial and axial velocities are zero due to the no-slip condition, while the tangential velocity varies linearly across the radius

$$u(r, 0) = u(r, L) = r\omega \tag{9}$$

$$v(r, 0) = v(r, L) = 0 \tag{10}$$

$$w(r, 0) = w(r, L) = 0. \tag{11}$$

At the centerline of the pipe ($r = 0$), the radial and tangential velocities, and the radial gradients of the pressure and axial velocity are zero

$$v = u = \frac{\partial p}{\partial r} = \frac{\partial w}{\partial r} = 0. \tag{12}$$

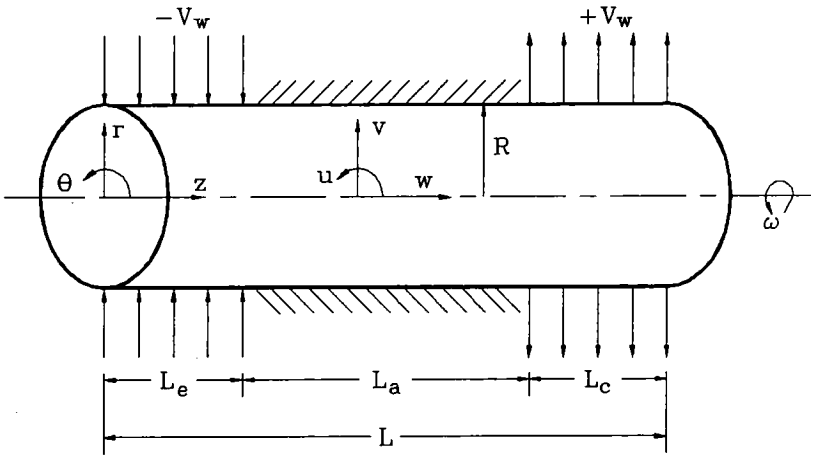

FIG. 1. The axially rotating heat pipe and coordinate system.

The pressure at the center of the evaporator end cap is set to a constant value (reference pressure)

$$p(0, 0) = p_0. \tag{13}$$

The shear stresses at the inner wall of the heat pipe are [13]:

$$\tau_{rz,w} = \mu\left(\frac{\partial w}{\partial r}\right)\bigg|_{r=R} \tag{14}$$

$$\tau_{r\theta,w} = \mu\left[r\frac{\partial}{\partial r}\left(\frac{u}{r}\right)\right]_{r=R}. \tag{15}$$

The solutions of the conservation equations and boundary conditions given above are presented in terms of the following dimensionless dependent variables:

$$p^* = \frac{(p-p_0)}{\rho \bar{W}^2}, \quad u^+ = \frac{u}{U_w}, \quad v^+ = \frac{v}{V_w}, \quad w^+ = \frac{w}{W_{avg}},$$

$$C_{f,r\theta} = \frac{2\tau_{r\theta,w}}{\rho U_w^2}, \quad C_{f,rz} = \frac{2\tau_{rz,w}}{\rho \bar{W}^2}.$$

The dimensionless independent variables and parameters are:

$$r^+ = \frac{r}{R}, \quad z^+ = \frac{z}{L},$$

$$Re_r = \frac{V_w R}{\nu}, \quad Ro = \frac{V_w}{\omega R}.$$

NUMERICAL METHODOLOGY

The solutions of the elliptic dimensional mass and momentum conservation equations (1)–(4) with the boundary conditions, (5)–(7), (9)–(13), were obtained using the control volume finite difference approach described by Patankar [14, 15]. The solution procedure is based on a line-by-line iteration method in the axial direction, and the Jacobi point-by-point procedure in the radial direction. The SIMPLEST method is employed for the momentum equations [16]. The pressure field is solved by the whole-field pressure correction algorithm derived by Markatos *et al.* [17]. The pressure field is first assumed and then the velocities are solved. The pressure correction equation is then solved using the mass errors that have been calculated during the sweep, and the other variables are updated accordingly. A new sweep will start until convergence is attained. Convergence of the solutions is ensured in two ways:

1. The sum of the absolute value of the residuals should decrease as the sweep number increases.
2. The spot values monitored during the iterations should approach constant values as the sweep number increases.

Sweep independence was ensured by monitoring the dependent variables at a location of maximum change as the number of sweeps increased until the solutions did not change by more than 0.1%, and the residuals of each equation was less than 10^{-6}. Grid independence was checked by systematically varying the number of cells in the r and z directions until an invariant solution was obtained. A change in the number of r–z cells from 40×80 to 60×120 resulted in a change in the dependent variables of less than 3%, so 40×80 uniform cells were used in all of the runs.

RESULTS AND DISCUSSION

A parametric study of the effects of radial Reynolds number and rotational speed on the vapor flow within an axially rotating heat pipe has been completed. Pressure, velocity, and shear stress profiles are presented for radial Reynolds numbers of 0.01, 4.0, and 20.0, and rotational speeds from 0 to 2800 r.p.m. The validity of the numerical code was verified by comparison with the numerical results of previous researchers. First, the laminar vapor pressure distribution of a stationary heat pipe ($Re_r = 0.01$, $N = 0$) was compared to the analytical solution given by Faghri and Parvani [6]. The code was then changed to simulate developing laminar flow from a stationary to a rotating tube, so that the results of Lavan *et al.* [18] ($Re = 20$, $\Gamma = 5.22$) could be reproduced. Finally, the numerical code was run for the case of fully-developed flow in a rotating pipe (Reich *et al.* [19]; $Re = 1000$). In all three cases, the results of the present numerical code were within 1.0% of the previous results.

Figures 2–4 present the dimensionless axial, radial, and tangential velocities across the radius for the full range of rotational speed at three different axial locations for the case of $Re_r = 0.01$. In these figures, (a), (b), and (c) correspond to $z^+ = 0.1$, 0.5, and 0.9, which are at the middle of the evaporator, adiabatic, and condenser sections. At $N = 0$ (stationary heat pipe), the fully-developed parabolic axial velocity found by Faghri and Parvani [6] is shown in Fig. 2 in all sections of the heat pipe. However, this profile changes significantly as the rotational speed increases. The centrifugal force tends to compress the fluid toward the pipe wall ($r^+ = 1$), so that the maximum velocity occurs away from the centerline, thus creating an annular main flow. At rotational speeds above $N = 1400$ r.p.m., the axial velocity near the centerline becomes negative, indicating a central core of reversed flow down the length of the heat pipe. This type of flow reversal was reported by Lavan *et al.* [18] for the case of developing flow from a rotating tube to a stationary tube. In the present case, flow reversal occurs due to the decrease of the pressure near the center of the heat pipe, and the increase in the momentum of the fluid from the angular velocity. The momentum of the annular main flow is such that the fluid is not completely removed by the suction in the condenser, so that the annular flow turns toward the

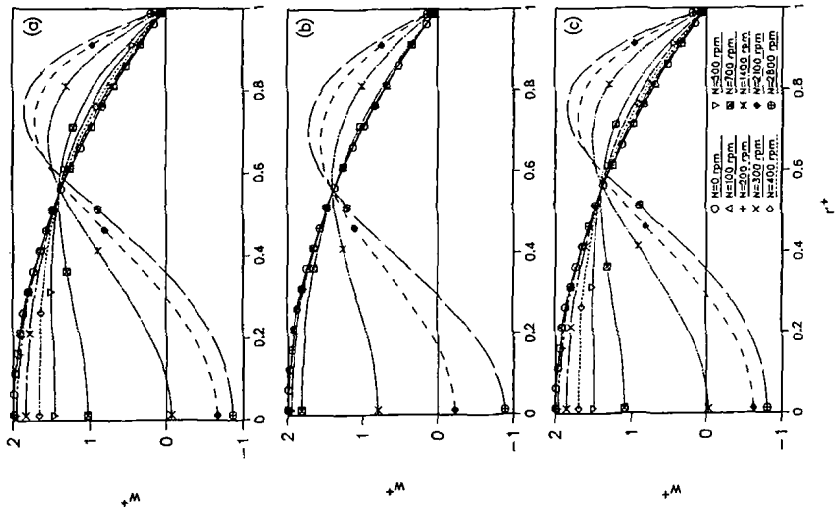

FIG. 2. Normalized axial velocity variation along the radius for $Re_t = 0.01$: (a) Evaporator mid-section ($z' = 0.1$); (b) Adiabatic mid-section ($z^+ = 0.5$); (c) Condenser mid-section ($z^+ = 0.9$).

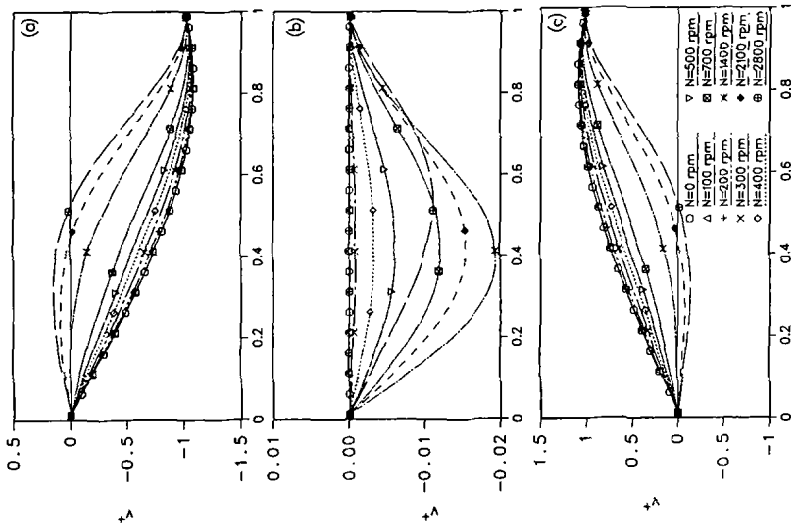

FIG. 3. Normalized radial velocity variation along the radius for $Re_t = 0.01$: (a) Evaporator mid-section ($z' = 0.1$); (b) Adiabatic mid-section ($z^+ = 0.5$); (c) Condenser mid-section ($z^+ = 0.9$).

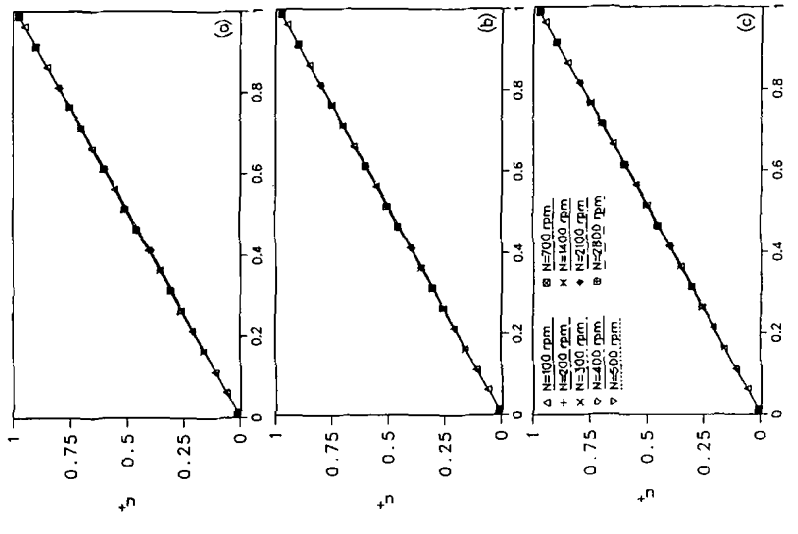

FIG. 4. Normalized tangential velocity variation along the radius for $Re_t = 0.01$: (a) Evaporator mid-section ($z^+ = 0.1$); (b) Adiabatic mid-section ($z^+ = 0.5$); (c) Condenser mid-section ($z^+ = 0.9$).

centerline in the condenser and becomes the central reversed flow.

Figure 3 presents the radial velocity down the length of the heat pipe. In Fig. 3(a), v^+ is negative in the evaporator at the pipe wall, indicating that fluid is being blown into the pipe. In Fig. 3(b), the velocity at the wall is zero, due to the adiabatic condition. In Fig. 3(c), the radial velocity at the wall is positive, showing suction from the pipe. At high rotational speeds, the radial velocity becomes positive close to the centerline of the pipe in the evaporator section, as shown in Fig. 3(a). This means that the fluid from the central reversed flow turns toward the annular main flow in the evaporator section. Similarly, the radial velocity near the centerline becomes negative in the condenser section, showing the flow turns from the annular main flow to the central reversed flow in the condenser. Therefore, the centrifugal force causes the fluid to circulate within the pipe such that part of the fluid passes by the condenser section without being drawn out.

Figure 4 presents the tangential velocity across the radius at different locations, which was nearly linear for the entire range of the rotational speed. The dimensional pressure distribution across the radius for $Re_r = 0.01$ is shown in Fig. 5. At low rotational speeds, the pressure is constant across the radius, as was found by Faghri and Parvani [6]. As the rotational speed increases, the pressure increases significantly across the radius due to the centrifugal force. In fact, for the case of $Re_r = 0.01$ with high rotational speeds, the pressure variation across the radius is several orders of magnitude higher than that along the axial length of the heat pipe. Figure 6(a) presents the dimensionless axial pressure variation at the centerline for $Re_r = 0.01$. At low rotational speeds, the direction of the flow is from the evaporator to the condenser. As the rotational speed increases, the pressure in the condenser becomes higher than that in the adiabatic and evaporator sections, indicating a reversal of flow near the centerline. Similar profiles occur for $Re_r = 4.0$ and 20.0, as shown in Figs. 6(b) and (c). In Fig. 6(c), for $N = 700$ r.p.m., the centerline pressure is negative from $0 \leqslant z^+ \leqslant 0.35$ and positive from $0.35 \leqslant z^+ \leqslant 1$. This means that the central reversed flow is present only in the region of $0.35 \leqslant z^+ \leqslant 1$. As the rotational speed increases, the extent of the central reversed flow increases until it fills the heat pipe.

The normalized axial velocity for $Re_r = 4.0$ is given in Fig. 7. Again, the reversed flow near the centerline is found in this case for $N > 1400$ r.p.m. at all axial locations down the length of the pipe. The radial velocity for $Re_r = 4.0$, shown in Fig. 8, is similar to that of $Re_r = 0.01$ (Fig. 3). The normalized tangential velocity for $Re_r = 4.0$ no longer varies linearly across the radius, as shown in Fig. 9. Near the pipe wall, the tangential velocity is not significantly affected by the rotational speed since the viscous effects of the wall dominate in that area. Away from the wall, however, the rotational speed dramatically affects the tangential velocity profile. The u^+ velocity in the evaporator section reaches a maximum which is greater than the velocity of the rotating wall, which indicates an increase in swirl in the evaporator section due to the blowing at the pipe wall. Alternately, the suction velocity in the condenser section decreases swirl.

Figure 10 presents the normalized axial velocity for $Re_r = 20.0$. Similar behaviors are seen as before, except that at low rotational speeds, the axial velocity reverses in the condenser section near the pipe wall. This phenomenon was also seen by Faghri and Parvani [6]. As the rotational speed increases, the momentum of the annular core overcomes the reversed flow at the wall, which then turns in the positive z direction. By comparing w^+ for $Re_r = 0.01$, 4.0, and 20.0, it can be seen that the maximum in the axial velocity at $N = 2800$ r.p.m. moves away from the pipe wall ($r^+ = 1$) in the evaporator section as the radial Reynolds number increases. In the condenser section, the maximum moves toward the pipe wall as Re_r increases. This means that the influence of the blowing or suction velocity at the wall changes the axial velocity profile more at higher radial Reynolds numbers. The normalized radial and tangential velocities are given in Figs. 11 and 12 for $Re_r = 20.0$.

Figure 13 presents the coefficient of friction at the wall in the r–z plane along the heat pipe length for $Re_r = 0.01$, 4.0, and 20.0. The results in the adiabatic section for the case of no rotation was compared to the Hagen–Poiseuille laminar friction law, $C_{f,rz} = 16/Re$, with agreement to within 1.0%. For $Re_r = 0.01$, Fig. 13(a), the magnitude of the friction coefficient increases in the evaporator section for a given rotational speed due to the increase in the axial velocity by mass injection. The friction coefficient also increases with rotational speed in the evaporator section due to the change in the axial velocity profile, as shown in Fig. 2(a). Since the gradient of the axial velocity at the wall becomes steeper with an increase in the rotational speed, the shear stress also increases. Similarly, in the condenser section, the friction coefficient decreases due to mass extraction for a given rotational speed, and increases at a particular location with the rotational speed.

Figure 13(a) also shows that a sudden discontinuity occurs at the end of the evaporator section when the pipe rotates because of the discontinuous blowing velocity boundary condition at the pipe wall. The magnitude of the friction coefficient decreases monotonically until the middle of the adiabatic section, where it again increases. The decrease in the magnitude of the friction coefficient is similar to that found by Imao *et al.* [20] for the hydrodynamic development length in a rotating pipe. Therefore, the decrease in $C_{f,rz}$ is due to the development of the axial profile in the adiabatic section. For low rotational speeds, $C_{f,rz}$ approaches the constant value of that for no rotation, which is expected as the axial velocity profile becomes fully developed. $C_{f,rz}$ increases between the middle of

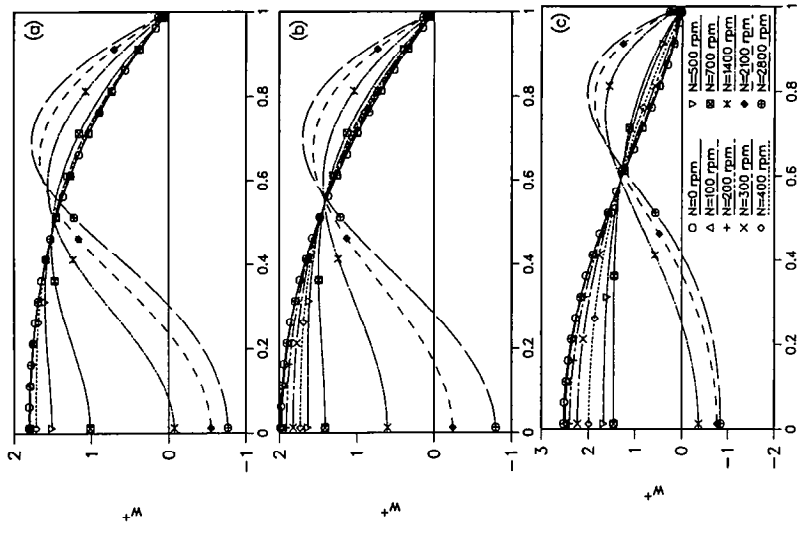

FIG. 7. Normalized axial velocity variation along the radius for $Re_r = 4.0$: (a) Evaporator mid-section ($z^+ = 0.1$); (b) Adiabatic mid-section ($z^+ = 0.5$); (c) Condenser mid-section ($z^+ = 0.9$).

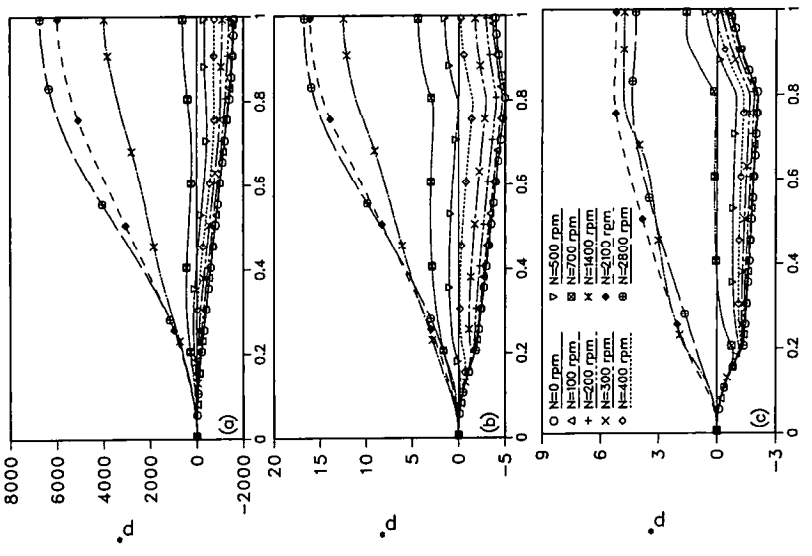

FIG. 6. Dimensionless pressure variation at the centerline along the length of the heat pipe for: (a) $Re_r = 0.01$; (b) $Re_r = 4.0$; (c) $Re_r = 20.0$.

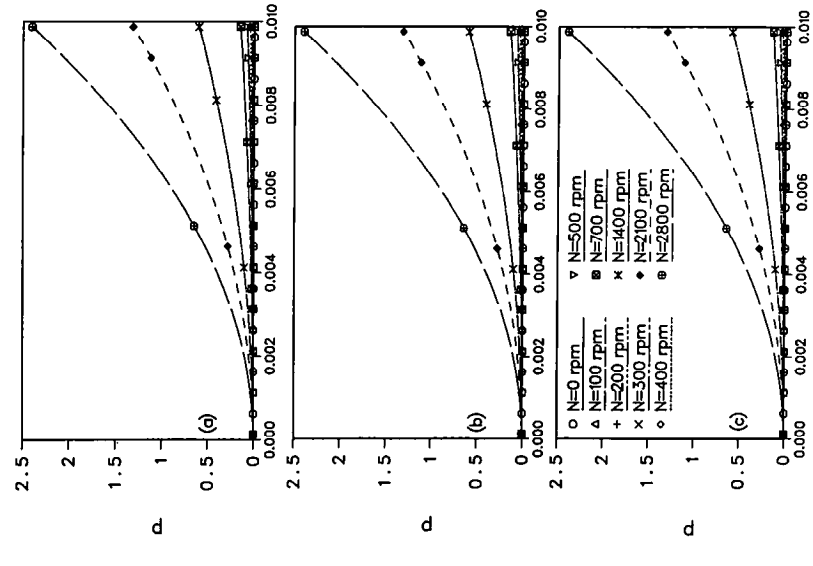

FIG. 5. Dimensional pressure variation along the radius for $Re_r = 0.01$: (a) Evaporator mid-section ($z^+ = 0.1$); (b) Adiabatic mid-section ($z^+ = 0.5$); (c) Condenser mid-section ($z^+ = 0.9$).

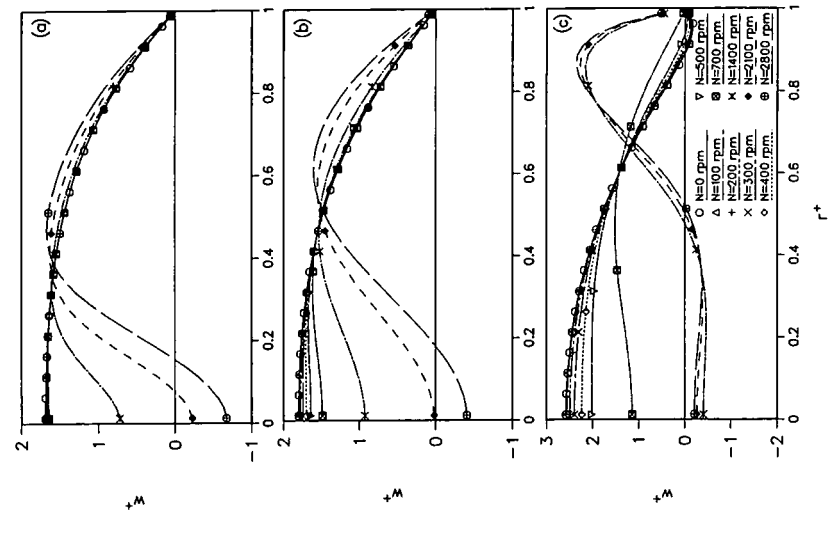

FIG. 10. Normalized axial velocity variation along the radius for $Re_r = 20.0$: (a) Evaporator mid-section ($z^+ = 0.1$); (b) Adiabatic mid-section ($z^+ = 0.5$); (c) Condenser mid-section ($z^+ = 0.9$).

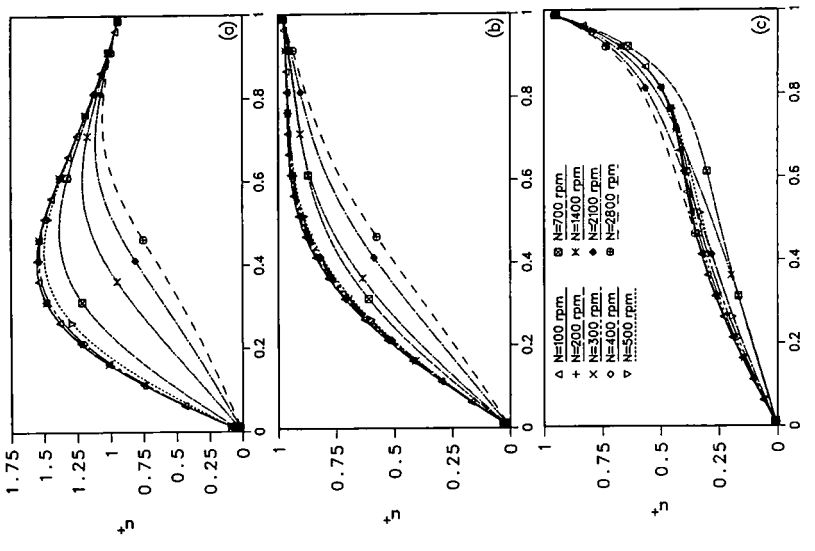

FIG. 9. Normalized tangential velocity variation along the radius for $Re_r = 4.0$: (a) Evaporator mid-section ($z^+ = 0.1$); (b) Adiabatic mid-section ($z^+ = 0.5$); (c) Condenser mid-section ($z^+ = 0.9$).

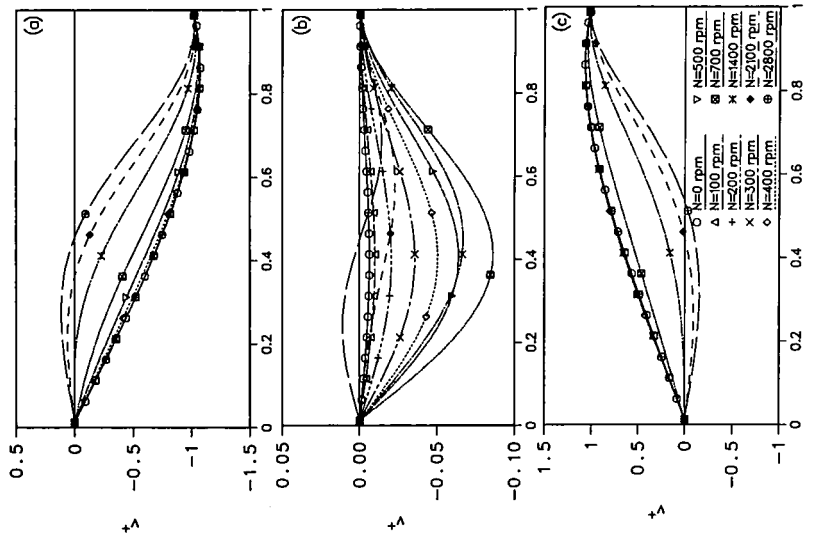

FIG. 8. Normalized radial velocity variation along the radius for $Re_r = 4.0$: (a) Evaporator mid-section ($z^+ = 0.1$); (b) Adiabatic mid-section ($z^+ = 0.5$); (c) Condenser mid-section ($z^+ = 0.9$).

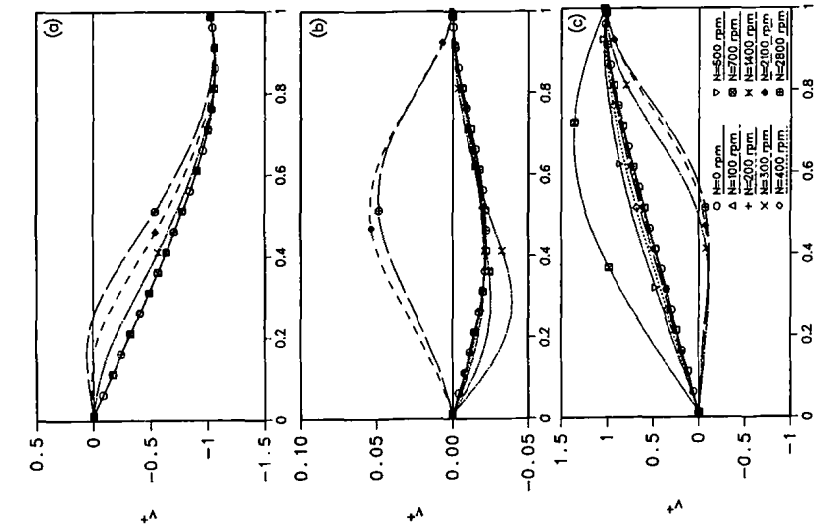

FIG. 11. Normalized radial velocity variation along the radius for $Re_t = 20.0$: (a) Evaporator mid-section ($z^+ = 0.1$); (b) Adiabatic mid-section ($z^+ = 0.5$); (c) Condenser mid-section ($z^+ = 0.9$).

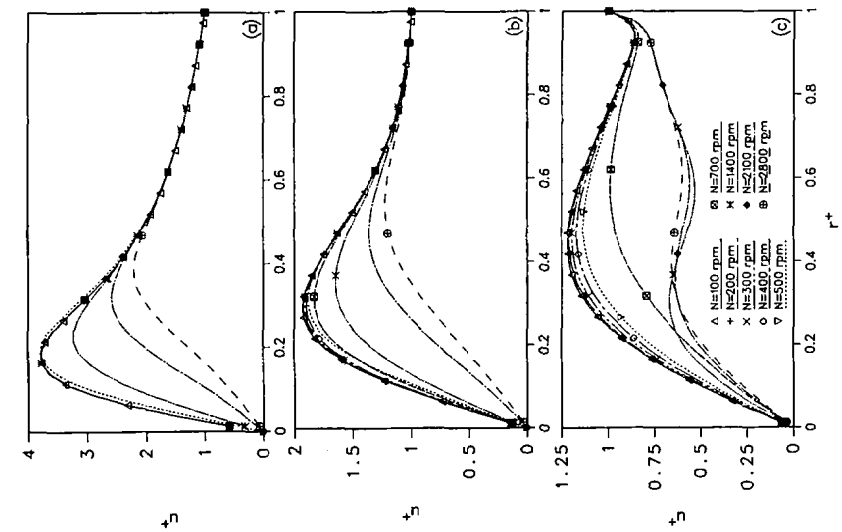

FIG. 12. Normalized tangential velocity variation along the radius for $Re_t = 20.0$: (a) Evaporator mid-section ($z^+ = 0.1$); (b) Adiabatic mid-section ($z^+ = 0.5$); (c) Condenser mid-section ($z^+ = 0.9$).

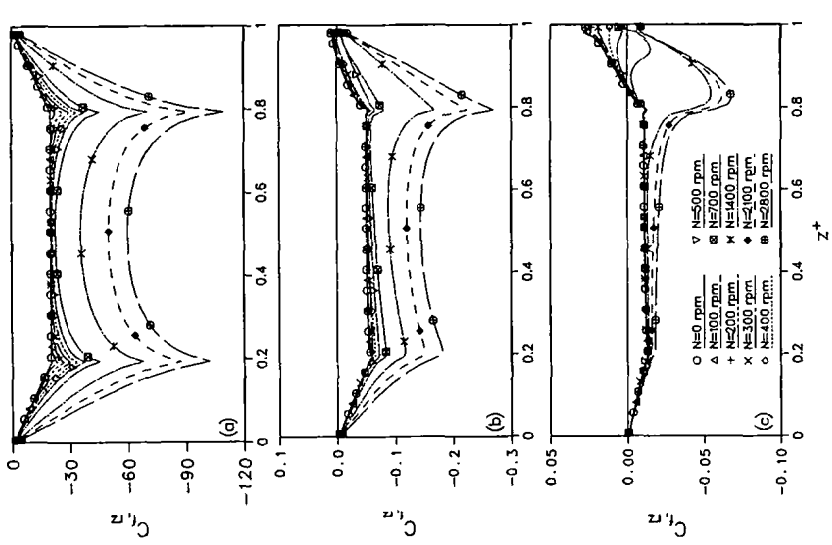

FIG. 13. Axial coefficient of friction variation along the length of the heat pipe for: (a) $Re_t = 0.01$; (b) $Re_t = 4.0$; (c) $Re_t = 20.0$.

the adiabatic section and the beginning of the condenser section. This behavior is more pronounced as the rotational speed increases. This phenomenon is caused by the influence of the downstream condenser section propagating upstream, which begins to change the axial velocity profile in the adiabatic section. If the adiabatic section was longer, $C_{f,rz}$ for $N = 2800$ r.p.m. would approach the fully-developed value more closely before increasing at the junction of the adiabatic and condenser sections. This shows that the downstream effects must be accounted for in the solution of this problem. Chen and Faghri [7] and Tien and Rohani [21] showed that for a stationary heat pipe with low radial Reynolds numbers, the partially parabolic conservation equations sufficiently represented the physics of the problem in comparison to the elliptic equations. For the rotating heat pipe, however, the fully elliptic conservation equations must be solved, even for radial Reynolds numbers as low as $Re_r = 0.01$.

As the radial Reynolds number increases, as seen in Figs. 13(b) and (c), $C_{f,rz}$ is not affected as greatly in the evaporator and adiabatic sections, since the blowing velocity becomes larger in relation to the tangential velocity of the wall (Ro increases). Also in Figs. 13(b) and (c), the coefficient of friction changes sign in the condenser section due to the flow reversal near the pipe wall at low rotational speeds. This is eliminated at higher speeds due to the momentum of the annular flow overcoming that of the reversed flow at the wall, as shown in Fig. 10(c). $C_{f,rz}$ decreases as Re_r increases because $C_{f,rz}$ is calculated by dividing the shear stress by the square of the mean axial velocity in the adiabatic section, which increases with radial Reynolds number. The magnitude of the r–z component of the shear stress is greatest in the condenser section in all cases.

Figure 14 presents the coefficient of friction at the wall in the r–θ plane, $C_{f,r\theta}$. In Fig. 14(a) ($Re_r = 0.01$), the coefficient of friction decreases in all sections of the rotating heat pipe as the rotational speed increases because $\tau_{r\theta}$ is nondimensionalized by U_w. In Fig. 14(b), $C_{f,r\theta}$ becomes negative in the evaporator and adiabatic sections due to the change in the slope of u^+ in that region (see Figs. 9(a) and (b)). In the condenser section, the coefficient of friction is positive, and its magnitude is greatest in this section in all cases.

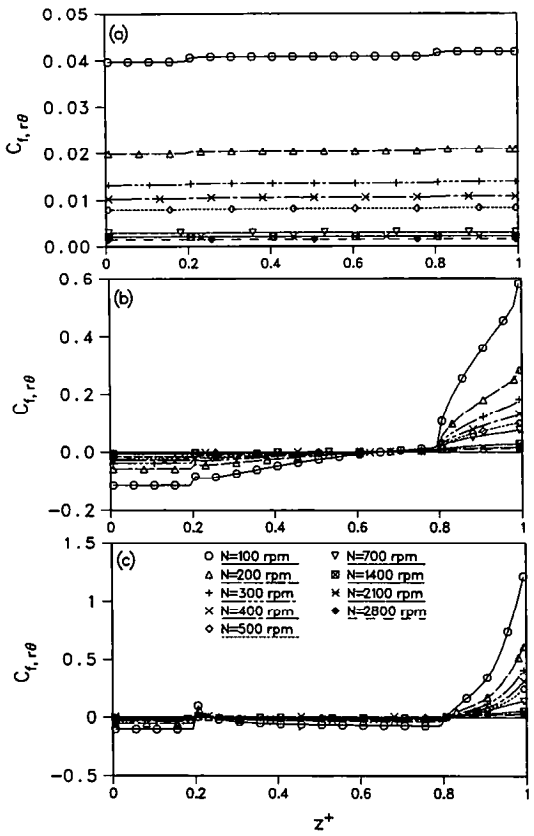

FIG. 14. Tangential coefficient of friction variation along the length of the heat pipe for: (a) $Re_r = 0.01$; (b) $Re_r = 4.0$; (c) $Re_r = 20.0$.

CONCLUSIONS

A parametric numerical analysis of axially rotating heat pipes has been carried out, with the following conclusions:

1. Rotation significantly changes the velocity profiles of the vapor flow within the heat pipe. A reversal of flow near the centerline of the pipe occurs due to the reduced pressure at that location. To capture this effect, the elliptic version of the conservation equations must be solved, instead of just the fully parabolic equations.

2. Unlike stationary heat pipes, the radial pressure distribution of the rotating heat pipe is no longer uniform, but more closely resembles a parabolic profile.

3. The flow reversal normally seen in stationary heat pipes at the wall for large heat rates ($Re_r > 2$) is eliminated at high rotational speeds due to the increased momentum of the annular main flow.

4. The tangential velocity is affected by the blowing or suction velocities at the pipe wall in the evaporator and condenser sections. This increases the swirl in the evaporator and decreases it in the condenser section.

5. The coefficient of friction in the r–z direction is significantly affected by rotation when the radial Reynolds number is low, because the effects of the condenser section propagate upstream. In all cases, the magnitudes of $C_{f,rz}$ and $C_{f,r\theta}$ are greatest in the condenser section.

6. The shear stress components at the wall, $\tau_{rz,w}$ and $\tau_{r\theta,w}$ increase with both rotational speed and radial Reynolds number. Therefore, neglecting the shear stress at the vapor–liquid interface of an axially rotat-

ing heat pipe may induce significant errors in a Nusselt-type analysis.

REFERENCES

1. P. D. Dunn and D. A. Reay, *Heat Pipes* (3rd Edn). Pergamon Press, Oxford (1982).
2. V. H. Gray, The rotating heat pipe—A wickless, hollow shaft for transferring high heat fluxes, *Proc. ASME/AIChE Heat Transfer Conf.*, Minneapolis, 1-5, ASME Paper No. 69-HT-19 (1969).
3. M. Groll, H. Krahling and W. D. Munzel, Heat pipes for cooling of an electric motor, *3rd Int. Heat Pipe Conf.*, 354–359 (1978).
4. P. J. Marto, Rotating heat pipes, *Proc. 14th ICHMT Symp.*, Dubrovnik, Yugoslavia, Paper no. 6 (1982).
5. F. Giessler, Ph. K. Sattler and F. Thoren, Heat pipe cooling of electrical machines, *6th Int. Heat Pipe Conf.*, 557 563 (1987).
6. A. Faghri and S. Parvani, Numerical analysis of laminar flow in a double-walled annular heat pipe, *J. Thermophys. Heat Transfer* **2,** 165–171 (1988).
7. M. M. Chen and A. Faghri, An analysis of the vapor flow and the heat conduction through the liquid-wick and pipe wall in a heat pipe with single or multiple heat sources, *Int. J. Heat Mass Transfer* **33,** 1945–1955 (1990).
8. T. C. Daniels and F. K. Al-Jumaily, Investigations of the factors affecting the performance of a rotating heat pipe, *Int. J. Heat Mass Transfer* **18,** 961–973 (1975).
9. W. Nusselt, Die oberflachen kondensation des wasserdampfes, *Z. Ver. dr. Ing.* **60,** 541 (1916).
10. P. J. Marto, Performance characteristics of rotating, wickless heat pipes, *2nd Int. Heat Pipe Conf.* **1,** 281–291 (1976).
11. T. C. Daniels and N. S. Al-Baharnah, Temperature and heat load distribution in rotating heat pipes, *3rd Int. Heat Pipe Conf.*, 170 176 (1978).
12. D. Salinas and P. J. Marto, Analysis of an internally finned rotating heat pipe, *Numer. Heat Transfer* **19,** 255–275 (1991).
13. E. N. Ganic, J. P. Hartnett and W. M. Rohsenow, *Handbook of Heat Transfer Fundamentals.* McGraw-Hill, New York (1985).
14. S. V. Patankar, *Numerical Heat Transfer and Fluid Flow.* McGraw-Hill, New York (1980).
15. S. V. Patankar, Elliptic systems: Finite-difference method I. In *Handbook of Numerical Heat Transfer* (Edited by W. J. Minkowycz *et al.*). Wiley, New York (1988).
16. D. B. Spalding, Mathematical modelling of fluid mechanics, heat transfer and chemical-reaction processes, A lecture course, CFDU report HTS/80/1, Imperial College, London (1980).
17. N. C. Markatos, M. R. Malin and G. Cox, Mathematical modeling of buoyancy-induced smoke flow in enclosures, *Int. J. Heat Mass Transfer* **25,** 63–75 (1982).
18. Z. Lavan, H. Nielsen and A. A. Fejer, Separation and flow reversal in swirling flows in circular ducts, *Physics Fluids* **12,** 1747–1757 (1969).
19. G. Reich, B. Weigand and H. Beer, Fluid flow and heat transfer in an axially rotating pipe—II. Effect of rotation on laminar pipe flow, *Int. J. Heat Mass Transfer* **32,** 563–574 (1989).
20. S. Imao, Q. Zhang and Y. Yamada, The laminar flow in the developing region of a rotating pipe, *JSME Int. J.*, Series II **32,** 10 (1989).
21. C. L. Tien and A. R. Rohani, Analysis of the effects of vapor pressure drop on heat pipe performance, *Int. J. Heat Mass Transfer* **17,** 61–67 (1974).